Lawrence Berkeley National Laboratory
FINAL SCIENTIFIC/TECHNICAL REPORT
DOE-LBNL-CH11231

Hydrogen Storage in Metal-Organic Frameworks

U.S. Department of Energy
Energy Efficiency and Renewable Energy
Fuel Cell Technologies Office

Award:	DE-NL0025051
Lead Recipient:	Lawrence Berkeley National Laboratory
Project Title:	Hydrogen Storage in Metal-Organic Frameworks
Principal Investigator:	Jeffrey Long
Team Members:	Martin Head-Gordon, Lawrence Berkeley Nat. Lab. Craig Brown, Nat. Inst. of Standards and Technology Anne Dailly, General Motors Corporation
Date of Report:	December 22, 2015
Date of Revised Report:	April 28, 2016
Reporting Period:	April 1, 2012-September 30, 2015

1 Table of Contents

2 Executive Summary

The design and characterization of new materials for hydrogen storage is an important area of research, as the ability to store hydrogen at lower pressures and higher temperatures than currently feasible with solid adsorbents would lower operating costs for small hydrogen fuel cell vehicles. In particular, metal-organic frameworks (MOFs) represent promising materials for use in storing hydrogen in this capacity. MOFs are highly porous, three-dimensional crystalline solids that are formed via linkages between metal ions (e.g., iron, nickel, and zinc) and organic molecules. MOFs can store hydrogen via strong adsorptive interactions between the gas molecules and the pores of the framework, providing a high surface area for gas adsorption and thus the opportunity to store hydrogen at significantly lower pressures than with current technologies. By lowering the energy required for hydrogen storage, these materials hold promise in rendering hydrogen a more viable fuel for light-duty vehicles, which is a highly desirable outcome given the clean nature of hydrogen fuel cells (water is the only byproduct) and the current state of global climate change resulting from the combustion of fossil fuels.

The work presented in this report is the result of collaborative efforts between researchers at Lawrence Berkeley National Lab (LBNL), the National Institute of Standards and Technology (NIST), and General Motors Corporation (GM) to discover novel MOFs promising for H_2 storage and characterize their properties. Described herein are several new framework systems with improved gravimetric and volumetric capacity to strongly bind H_2 at temperatures relevant for vehicle storage. These materials were rigorously characterized using neutron diffraction, to determine the precise binding locations of hydrogen within the frameworks, and high-pressure H_2 adsorption measurements, to provide a comprehensive picture of H_2 adsorption at all relevant pressures. A rigorous understanding of experimental findings was further achieved via first-principles electronic structure calculations, which also supported synthetic efforts through predictions of additional novel frameworks with promising properties for vehicular H_2 storage. The results of the computational efforts also helped to elucidate the fundamental principles governing the interaction of H_2 with the frameworks, and in particular with exposed metal sites in the pores of these materials.

Significant accomplishments from this project include the discovery of a metal-organic framework with a high H_2 binding enthalpy and volumetric capacity at 25 °C and 100 bar, which surpasses the metrics of any other known metal-organic framework. Additionally this material was designed to be extremely cost effective compared to most comparable adsorbents, which is imperative for eventual real-world applications. Progress toward synthesizing new frameworks containing multiple open coordination sites is also discussed, and appears to be the most promising future direction for hydrogen storage in these porous materials.

3 Accomplishments

Over the course of the award period, researchers at LBNL, NIST, and GM successfully accomplished a number of key objectives for the development of new sorbent materials optimized for hydrogen storage. A number of tasks and milestones were laid out at the beginning of the project and in the Annual Operating Plans. The actual performance against the stated milestones is summarized in Table 1.

Table 1: Milestones and Deliverables

Deliverables	Actual Performance
Task 1: Synthesis and Characterization of Metal-Organic Frameworks	
Go/No-go (03/31/13) Demonstration of the ability to prepare 5 mixed functionality ligands allowing for the post-synthetic insertion of metal cations.	**Completed (10/01/12)** 7 ligands containing both carboxylate and pyridine/phenol binding sites have been prepared
Go/No-go (03/31/13) Development of *in silico* screening techniques for calculating opposing pore surface distances.	**Completed (06/30/12)** Software completed
Go/No-go (03/31/13) Preparation of two new MOFs containing coordinatively-unsaturated high-valent cations.	**Completed (03/31/13)** Framework with open Ti^{3+} sites has been synthesized
Go/No-go (03/31/14) Synthesis of MOFs exhibiting reversible excess H_2 uptake greater than 2.5 wt %	**92% Completed (03/31/14)** Mg_2(dobpdc) has an uptake of 2.3 wt%; larger pore, less-dense analogues would likely meet the 2.5 wt% target
Go/No-go (03/31/14) Preparation of a high-valent MOF with an initial H_2 adsorption enthalpy greater than 12 kJ/mol.	**Completed (03/31/14)** Ni_2(*m*-dobdc) displays H_2 binding enthalpy of −13.7 kJ/mol
Go/No-go (03/31/14) Synthesis of new MOFs with the multifunctional ligands prepared in year 1	**Completed (03/31/14)** 3 bipyridine-MOFs synthesized
Go/No-go (03/31/14) Demonstration of the post-synthetic insertion of metals into the open chelate sites of these new materials	**Completed (03/31/14)** Single crystal diffractions shows binding of M^{2+} to the bipy sites
Go/No-go (03/31/14) Preparation of at least two MOFs with the optimal 7 Å between opposing pore surfaces as predicted with *in silico* screening techniques	**Completed (03/31/14)** 3 dicarboxylate MOFs synthesized with optimal pore size
Go/No-go (05/31/15)	**90% Completed (05/31/15)**

Deliverables	Actual Performance
Demonstration of a metal-organic framework with an initial H_2 adsorption enthalpy greater than the current record of 15.1 kJ/mol **Go/No-go (05/31/15)** Synthesis of a metal-organic framework with reversible excess hydrogen uptake greater than 4.5 wt % at 298 K **Progress Measure (09/30/15)** Complete the in-depth characterization of the H_2 storage properties of Ni_2(m-dobdc) **Milestone (09/30/15)** Synthesis and characterization of a MOF containing metal sites that can adsorb two or more H_2 molecules	A binding enthalpy of 13.7 kJ/mol was achieved in Ni_2(*m*-dobdc), which we believe to be the highest binding enthalpy in a MOF **60% Completed (05/31/15)** The M_2(dobpdc) series (M_2(dobdc) with two phenyl rings in the ligand) will most likely approach this at high pressures, but the focus on storage was switched to volumetric during the course of this project **Completed (09/30/15)** Ni_2(*m*-dobdc) evaluated fully to determine optimal temperature swing process to maximize volumetric H_2 usable capacity and determined to be the top performing MOF for high-pressure storage capacity **50% Completed (09/30/15)** Several metal-organic frameworks with more than one open metal site were synthesized, but the interaction with multiple H_2 molecules is yet to be shown
Task 2: Characterization of Framework-H_2 Interactions **Milestone (06/30/13)** Demonstrated ability to locate and uncover detailed descriptions of high-enthalpy H_2 binding sites in high-valent MOFs via neutron diffraction **Milestone (03/31/14)** Demonstrate that improved understanding of MOF-H_2 interactions through inelastic neutron scattering experiments and new approaches to calculate observed spectra provide new insight into the governing physics of adsorption in porous media **Progress Measure (03/31/15)** Demonstrate the use of quasielastic neutron scattering to help understand the roles of diffusion and entropy in H_2 binding to MOFs for the most interesting systems synthesized by Long	**Completed (06/30/13)** Diffraction measurements on pyridine and M_2(dobdc) variants performed. Analysis underway **Completed (07/01/14)** Inelastic neutron scattering measurements carried out on H_2 in M_2(dobdc) variants **95% Completed (03/31/15)** Quasi-elastic neutron scattering was used to characterize Hydrogen (D_2) diffusion behavior in Co_2(*m*-dobdc) and Ni_2(*m*-dobdc)
Task 3: First-Principles Calculations of Hydrogen Binding Enthalpies **Milestone (03/31/13)** Demonstration of a correlation between calculated and experimentally observed H_2 binding affinities as well as usefulness in facilitating design of new materials **Milestone (12/31/13)** Demonstrate the ability to determine H_2-metal	**Completed (03/31/13)** Calculated H_2 binding parameters agree with experimental values **Completed (12/31/13)** Demonstrated for Ca^{2+}, Mg^{2+}, Ni^{2+}, and Al^{3+} halides

Deliverables	Actual Performance
interactions in model systems containing low-coordinate metal cations	
Progress Measure (12/31/14) Demonstrate the ability to determine H_2-metal interactions in realistic systems containing low-coordinate metal cations	**Completed (12/31/13)** Demonstrated the ability to predict H_2 binding trends in M_2(*m*-dobdc) in agreement with experimentally measured values
Progress Measure (03/31/15) Pre-screen optimal metal-organic framework targets by identification of systems that produce an H_2 binding enthalpy greater than 20 kJ/mol	**Completed (03/31/15)** The catechol ligand, metalated by a magnesium ion, was shown to have a binding enthalpy of ~20 kJ/mol. The same metalated ligand is expected to adsorb up to four H_2 molecules
Task 4: High-Pressure H_2 Adsorption Measurements	
Milestone (03/31/13) Demonstrate the ability to accurately measure H_2 adsorption in MOFs at 298 K and pressures up to 350 bar	**Completed (03/31/13)** High-pressure system installed and some benchmark samples measured
Milestone (03/31/14) Demonstration of a correlation between high-pressure measurements and theoretical and spectroscopic predictions	**Completed (03/31/13)** Correlation demonstrated for several M_2(dobdc) variants
Milestone (6/30/14) Demonstrate the ability to measure H_2 adsorption in a test material up to 10 cycles at 298 K	**Completed (6/30/14)** Demonstrated for Ni_2(*m*-dobdc)
Milestone (9/30/14) Demonstrate the ability to measure H_2 adsorption in a test material up to 10 cycles at temperatures relevant to use in onboard vehicle applications	**Completed (9/30/14)** Successfully demonstrated integrity of adsorption capacity of Ni_2(*m*-dobdc) over 10 cycles at 40 °C

4 Project Activities

4.1 Task 1: Synthesis and Characterization of Metal-Organic Frameworks

The goals of this project were many, with an emphasis on improving the capacity of metal-organic frameworks (MOFs) for H_2 storage. Multiple methods were used to address this goal. Early on in the project, attempts were made at identifying MOFs with an optimal distance between pore surfaces for high H_2 uptake. Though this method is an established strategy for identifying metal-organic frameworks with high H_2 capacities, most materials that were studied based on this criterion did not exhibit high uptake of the gas. An example of these calculations is shown in Figure 1. Three optimal metal-organic frameworks predicted by this screening program exhibited only low H_2 uptake in high-pressure adsorption isotherms, however (Figure 2, see Go/No-go #8). Thus, it was decided that a more important design parameter is accessible strong adsorption sites within the framework pores, and the majority of the work presented herein is based on this approach. With an eye toward eventual use of these materials for H_2 storage in vehicles, an emphasis was also placed on the discovery of materials exhibiting a high *volumetric* density of H_2. Indeed, this characteristic is significantly more important to on-board H_2 storage in vehicles than *gravimetric* capacity, as volume limitations are more crucial than weight limitations when designing a tank that will fit into a vehicle. Therefore, while gravimetric capacity and volumetric capacity were both considered in the project, overall material performance was evaluated primarily on the basis of volumetric capacity (and also binding enthalpy).

Additional efforts included synthesis of the MOF Ti-MIL-101 with Ti^{3+} open metal sites. This material exhibited a high Langmuir surface area of 3050 m^2/g and O_2 isotherms indicated that at least 60% of the open metal coordination sites were accessible. In spite of these attributes, the material exhibited poor H_2 uptake and therefore it was not pursued further.

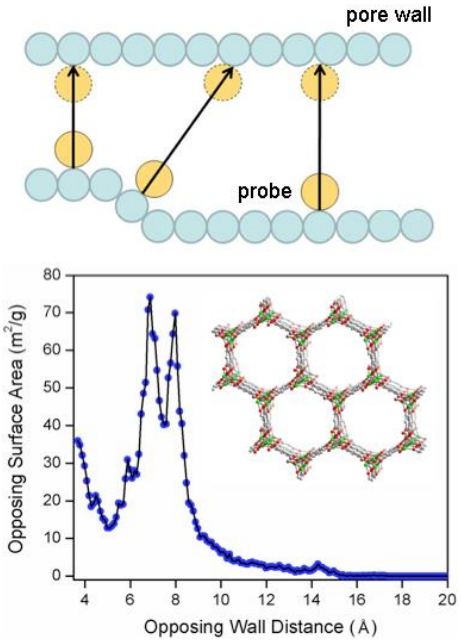

Figure 1. (Top) Schematic illustrating the opposing surface area calculations. Probe molecules (yellow) are inserted at various points along the structure surface and moved normal to the surface until a collision with the opposing wall is detected (dotted yellow). (Bottom) Portion of the crystal structure of $Mg_2(dobdc)$ ($dobdc^{4-}$ = 2,5-dioxido-1,4-benzenedicarboxylate) and its opposing surface area distribution plot (3.68 Å diameter probe molecule and 0.1 Å step size).

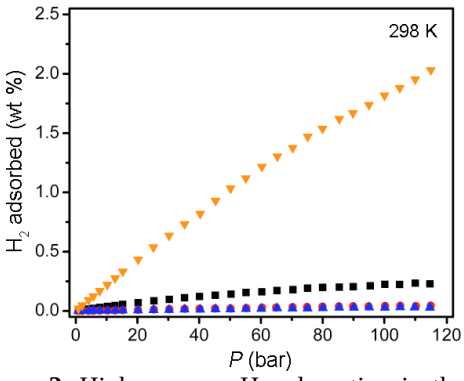

Figure 2. High-pressure H_2 adsorption isotherms collected for $Mg_2(dobdc)$ (yellow), Mg(ndc) (black, ndc^{2-} = 1,4-naphthalenedicarboxylate), Co(bdc)(dabco) (red, bdc^{2-} = 1,4-benzenedicarboxylate, dabco = 1,4-diazabicyclo[2.2.2]octane), and Cu(bdc)(dabco) (blue).

Mn-BTT

Initially, the $M_3[(M_4Cl)_3(BTT)_8]_2$ (M-BTT; BTT^{3-} = 1,3,5-benzenetristetrazolate, M = Cu, Mn, Fe, Zn) structure type was evaluated in a combined experimental and theoretical study. The M-BTT materials possess open metal coordination sites within the pores of the framework, which are the primary binding sites for H_2 as demonstrated through neutron diffraction studies. The thermodynamics of this interaction were studied via gas adsorption experiments and *in situ* infrared spectroscopy experiments and revealed that the binding enthalpies in the Fe-BTT and Mn-BTT analogs approached the record of –15.1 kJ/mol in a metal-organic framework (although this was proven to be an unreliable value, see below). The isosteric heat of adsorption plots, calculated from gas adsorption isotherms, are shown in Figure 3. Theoretical calculations were also found to be in close agreement with the experimental data (Section 4.3), confirming that the theoretical model is able to accurately describe the binding environments for H_2 within the M-BTT structure type. This result highlighted the importance of performing experimental and theoretical experiments in tandem to fully understand and predict the properties associated with H_2 binding in a given system. We also carried out substitutions within the metal cluster by either changing the metal ion or the anion within the cluster (i.e., F^-, Cl^-, Br^-) and found that the configuration of this cluster unit indeed plays an important role in determining the affinity of this framework for H_2. However, due to the explosive nature of these materials, further synthetic efforts were abandoned. Computational details for the anion-exchanged materials are provided in Section 4.3 of this report.

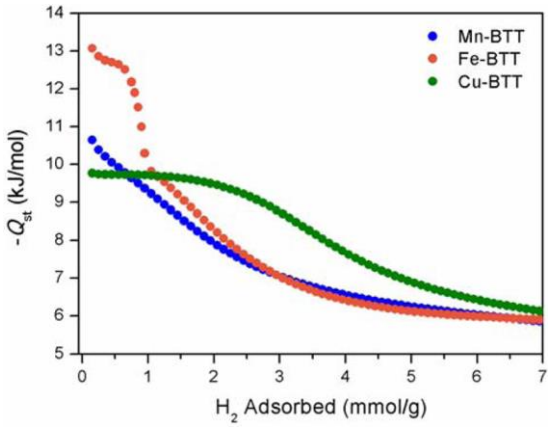

Figure 3. Isosteric heat of adsorption plots for Mn-, Fe-, and Cu-BTT. The high binding enthalpies at low loadings of H_2 are the result of the open metal coordination sites at the metal clusters.

M_2(dobpdc)

The M_2(dobpdc) ($dobpdc^{4-}$ = 4,4′-dioxidobiphenyl-3,3′-dicarboxylate; M = Mg, Mn, Fe, Co, Ni, Zn) series of frameworks also exhibits open-metal coordination sites and was studied for its high-pressure H_2 adsorption capacity. M_2(dobpdc) features the same weak-field, five-coordinate oxo-donor environment around the coordinatively unsaturated metal centers as in the well-known M_2(dobdc) structure type, but it possesses larger pores than the latter due to the expansion of the linker size by addition of one phenyl group (Figure 4). H_2 adsorption isotherms were measured in the full M_2(dobpdc) series at 77 K and 87 K in order to determine the binding enthalpy of H_2 in the pores of each analog. Low-loading isosteric

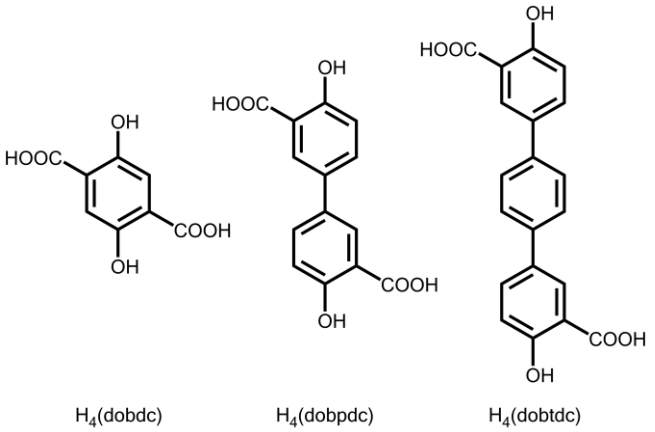

Figure 4. Structures of the ligands H_2(dobdc), H_2(dobpdc), and H_2(dobtdc), discussed in this report.

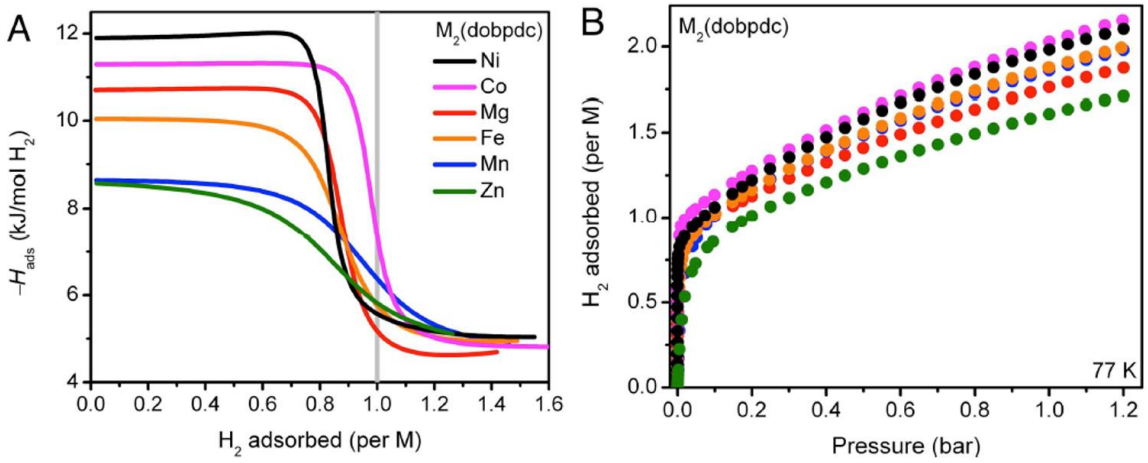

Figure 5. (A) Isosteric heats of adsorption plotted as a function of the amount of H_2 adsorbed for M_2(dobpdc). (B) Equilibrium H_2 adsorption isotherms for M_2(dobpdc) at 77 K.

heats of adsorption (representing the H_2 binding enthalpy at the open metal centers) were calculated from these isotherms and yielded binding enthalpies in the range of –8.8 to –12.0 kJ/mol with the trend Zn < Mn < Fe < Mg < Co < Ni (Figure 5). High-pressure adsorption isotherms at 25 °C indicated enhanced gravimetric uptakes compared to the M_2(dobdc) analogs, which can be attributed to the higher surface area and larger pores of the expanded analog. The determined gravimetric uptake of 2.3 wt% at 1.2 bar and 77 K in Mg(dobpdc) is quite high and could be increased further if the pores of the material were further expanded or the isotherms were measured at higher pressures (Section 4.4). It should be noted, however, that these larger pores contribute adversely to the goal of maximizing material volumetric capacity. Thus it is evident that it is desirable to pursue both high surface area materials, to improve gravimetric capacity, and materials with a high density of coordinatively unsaturated metal centers, to improve volumetric capacity.

Improved H_2 Adsorption in M_2(*m*-dobdc)

In order to optimally tune the chemistry in M_2(dobdc) for enhanced H_2 adsorption without sacrificing volumetric capacity, we synthesized and characterized the new series of metal-organic frameworks M_2(*m*-dobdc) (M = Mg, Mn, Fe, Co, Ni; *m*-dobdc^{4-} = 4,6-dioxido-1,3-benzenedicarboxylate, Figure 6). Notably, the *m*-dobdc^{4-} ligand is a structural isomer of the dobdc^{4-} ligand within the parent M_2(dobdc). In particular, *m*-dobdc^{4-} possess carboxylate groups that are meta to each other rather than para as in dobdc^{4-} (see Figure 4 for H_2(dobdc)). The resulting M_2(*m*-dobdc) material is also a structural isomer of the M_2(dobdc) framework while exhibiting different connectivity, due to the different placement of the carboxylate functionalities, and ultimately a different MOF structure. A substantial benefit of targeting this material for H_2 storage is that it represents a low-cost alternative to M_2(dobdc). Indeed the ligand can be synthesized in a solvent-free reaction from cheaply available resorcinol,

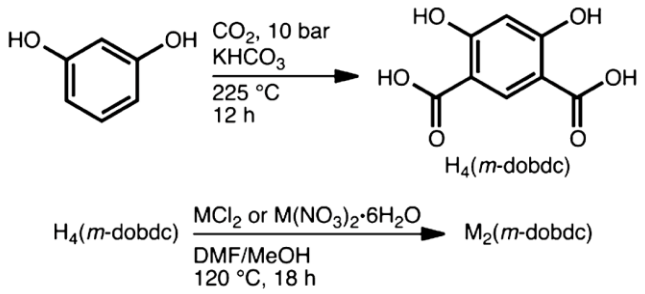

Figure 6. Synthesis of H_4(*m*-dobdc) and M_2(*m*-dobdc), starting from the inexpensive compound resorcinol.

$KHCO_3$, and CO_2. The H_2 storage properties of the M_2(*m*-dobdc) series were heavily investigated over the course of this project.

Gratifyingly, M_2(*m*-dobdc) exhibits significantly improved H_2 binding enthalpies when compared to the parent M_2(dobdc) frameworks for the Mn, Fe, Co, and Ni analogs. This result can be rationalized in part by the greater positive charge on the open metal coordination sites within M_2(*m*-dobdc), which lead to experimental isosteric heats of adsorption that are ~1.0 kJ/mol higher on average than for M_2(dobdc) (Figure 7).

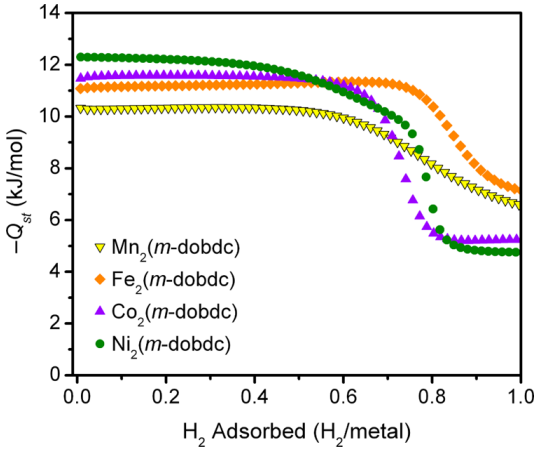

Figure 7. H_2 isosteric heat of adsorption plots for the M_2(*m*-dobdc) series of frameworks, as a function of the amount of gas adsorbed.

This stronger binding in the M_2(*m*-dobdc) series was also verified through *in situ* H_2-dosed infrared spectroscopy experiments. Both the Co_2(*m*-dobdc) and Ni_2(*m*-dobdc) variants exhibited H_2 stretching frequencies that were shifted to lower values (lower energy) as compared to the Co_2(dobdc) and Ni_2(dobdc) analogs. Additionally, variable temperature *in situ* H_2-dosed infrared spectroscopy was used to calculate site-specific binding enthalpies. From this work, the Ni_2(*m*-dobdc) analogue was determined to have the highest H_2 binding enthalpy of any reported MOF with a value of –13.7 kJ/mol (Figure 8). Previous work reported a slightly higher binding enthalpy of –15.1 kJ/mol for a cobalt(II) MOF, although this value was determined to be unreliable due to poor isotherm fits, which led to a significantly higher calculated isosteric heat of adsorption than was reasonable.[1]

Further studies on the M_2(*m*-dobdc) series sought to elucidate optimal conditions for storing H_2 at pressures up to 100 bar and temperatures closer to ambient temperature, which are relevant conditions for on-board storage in a light-duty vehicle. Temperature-swing processes can also be considered in such a study, as the usable capacity of H_2 adsorbed at 100 bar at a given temperature could be improved by desorbing to 5 bar pressure at a different, higher, temperature. The amount of H_2 adsorbed between 100 bar and 5 bar is defined by the DOE as the usable capacity of the MOF and is the amount that can be utilized in a typical system.

In order to determine the best conditions and materials for storing H_2, pristine samples of several MOFs (Co_2(*m*-dobdc), Ni_2(*m*-dobdc), Co_2(dobdc), and Ni_2(dobdc)) were synthesized and tested for their high-pressure H_2 capacities at nine different temperatures: 100, 75, 50, 25, 0, –25, –40, –50, and –75 °C (Figure 9). Such a wide temperature sampling can be used to determine both uptake at a given temperature and optimal temperature swings to maximize usable H_2 capacity. The results for these materials are shown in Figure 9 and, in line with the *in situ* infrared experiments above, Ni_2(*m*-dobdc) is again the top-performing material as evaluated by multiple temperature swing processes. This material has a total usable capacity of 11.0 g/L at 25 °C with no temperature swing, which is superior to any other

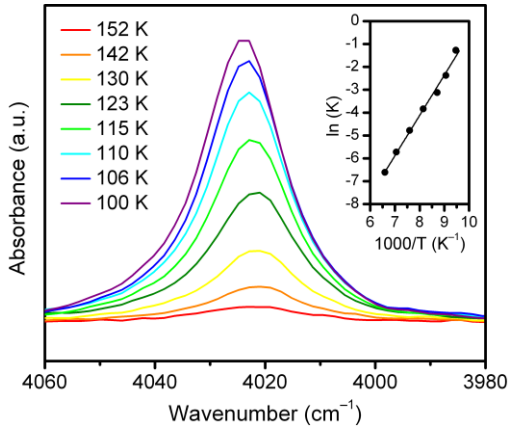

Figure 8. Variable-temperature infrared spectra of Ni_2(*m*-dobdc); the inset shows the van't Hoff plot, used to extract the H_2 enthalpy and entropy change upon adsorption to the open metal site.

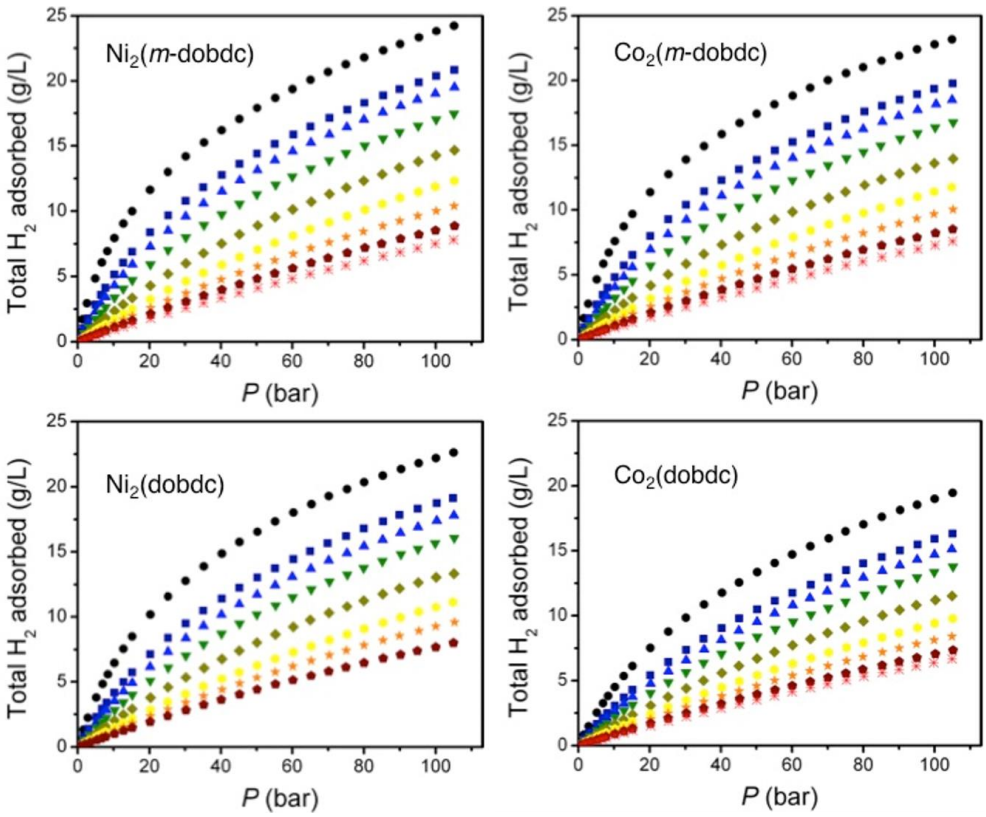

Figure 9. High-pressure H_2 isotherms for Ni_2(*m*-dobdc), Co_2(*m*-dobdc), Ni_2(dobdc), and Co_2(dobdc). The temperatures are –75 °C (black circles), –50 °C (navy squares), –40 °C (blue triangles), –25 °C (green downward-pointing triangles), 0 °C (gold diamonds), 25 °C (yellow circles), 50 °C (orange stars), 75 °C (dark red pentagons), and 100 °C (red crosses). The total capacity is calculated based on the single crystal density of each material.

known MOF. Additionally, for temperature swing processes from –40 °C to 25 °C and –75 °C to 25 °C, the usable capacity was determined to be 18.2 g/L and 23.0 g/L, respectively. These values are each significantly higher than the usable capacities for the other measured materials. Table 1 presents a comparison of the total volumetric usable capacities for each material with the relevant temperature swings.

Table 1. Total volumetric usable capacities for H_2 for various temperature swings (assuming single-crystal density); all units are in g/L.

Swing	Ni_2(*m*-dobdc)	Ni_2(dobdc)	Co_2(*m*-dobdc)	Co_2(dobdc)
25 °C, no swing	11.0	10.0	10.5	8.8
–75 °C, no swing	19.0	18.4	18.2	16.5
–40 to 25 °C	18.2	16.6	17.3	14.0
–75 to 25 °C	23.0	21.4	21.9	18.3

Binding Two H_2 Molecules per Metal

Another significant synthetic thrust of this project was to target metal-organic frameworks with the ability to bind multiple H_2 molecules at a single metal site. The above results showed that the open metal coordination sites are the primary sites of interaction for H_2 in multiple metal-organic frameworks. Thus, by increasing the density of open coordination sites in the pore, for example by exposing multiple coordination sites per metal center, the volumetric density of H_2 in a MOF should significantly increase. Our main strategy for engineering multiple metal coordination sites

was to synthesize MOFs with chelating sites in the pores that could subsequently bind non-structural metal cations through post-synthetic metalation. Subsequent desolvation of the metal centers could then result in multiple exposed coordination sites on each metal with which H_2 molecules could interact.

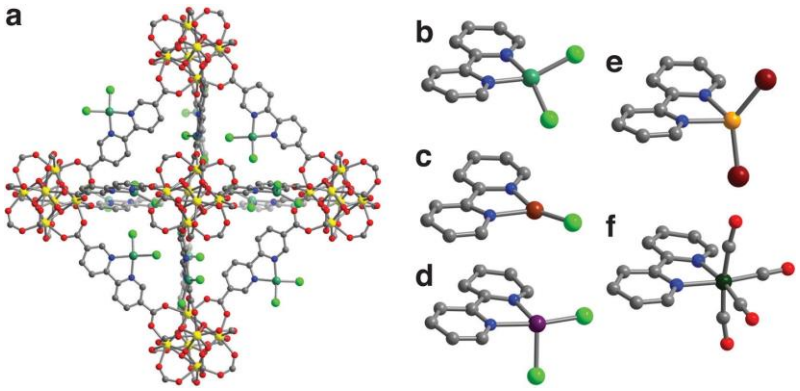

Figure 10. Structure of the metalated UIO-67-bpydc (a) showing the partial crystal structures of several of the incorporated metals Cu^{II} (b), Cu^{I} (c), Co^{II} (d), Fe^{II} (e), and Cr^{IV}(f).

In targeting the above approach we synthesized $Zr_6O_4(OH)_4(bpydc)_6$ (UIO-67-bpydc; $bpydc^{2-}$ = 2,2′-bipyridine-5,5′-dicarboxylate), which is a promising candidate from the UIO-67 family. This material contains open bipyridine sites that readily react with different metal salts to form the corresponding metalated frameworks. It was anticipated that the metalation of this material and subsequent activation would yield framework metal-bipyridine complexes with multiple available coordination sites. $Zr_6O_4(OH)_4(bpydc)_6$ was metalated with a variety of sources including $PdCl_2$, $CuCl_2$, $FeBr_2$, $FeCl_2$, $Cr(CO)_4$, $CoCl_2$, and CuCl (Figure 10). Single crystal X-ray diffraction revealed that the bipyridine-coordinate metal center distorts from square planar for all the synthesized variants (Figure 10), however, potentially reducing the number of anticipated H_2 binding sites available.

All of the metalated materials were characterized using low-pressure H_2 adsorption measurements and this data was compared to that of the bare, unmetalated framework (Figure 11). Notably, several of the post-synthetically modified samples exhibited higher H_2 uptake than the bare framework, with the $PdCl_2$- and $CuCl_2$-metalated samples showing the greatest increase in capacity. Based on the excess adsorption at 77 K and 1 bar it was estimated that 2.6 and 1.5 molecules coordinate per metal center in the $PdCl_2$ and $CuCl_2$ samples, respectively. (This very simple estimate is made based on the fact that the units of excess adsorption are millimoles per gram of material. Thus, based on the measured molar quantity of H_2 adsorbed per gram, the sample mass, and the density of metal sites in the framework, the number of adsorbed H_2 can be determined at a given pressure and temperature). This promising result prompted us to investigate this interaction further via D_2-dosed powder neutron

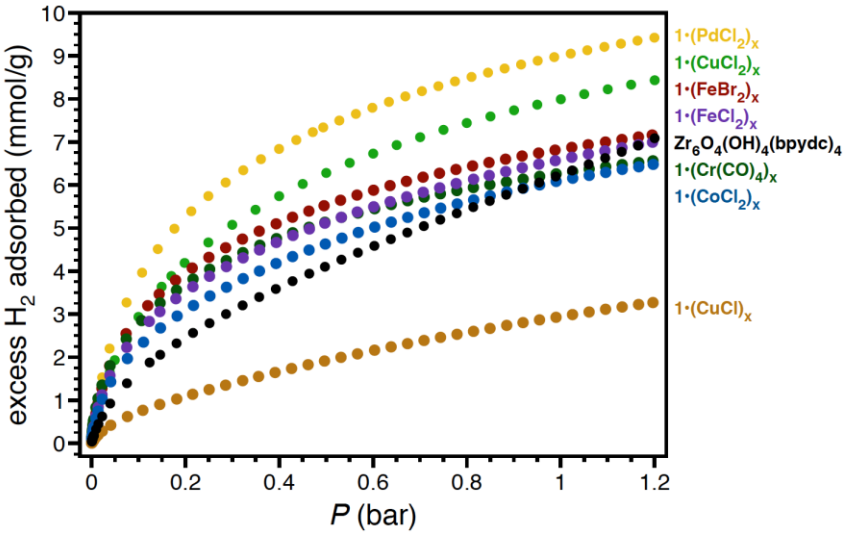

Figure 11. H_2 adsorption for the metalated UIO-67-bpydc samples as compared to the bare framework.

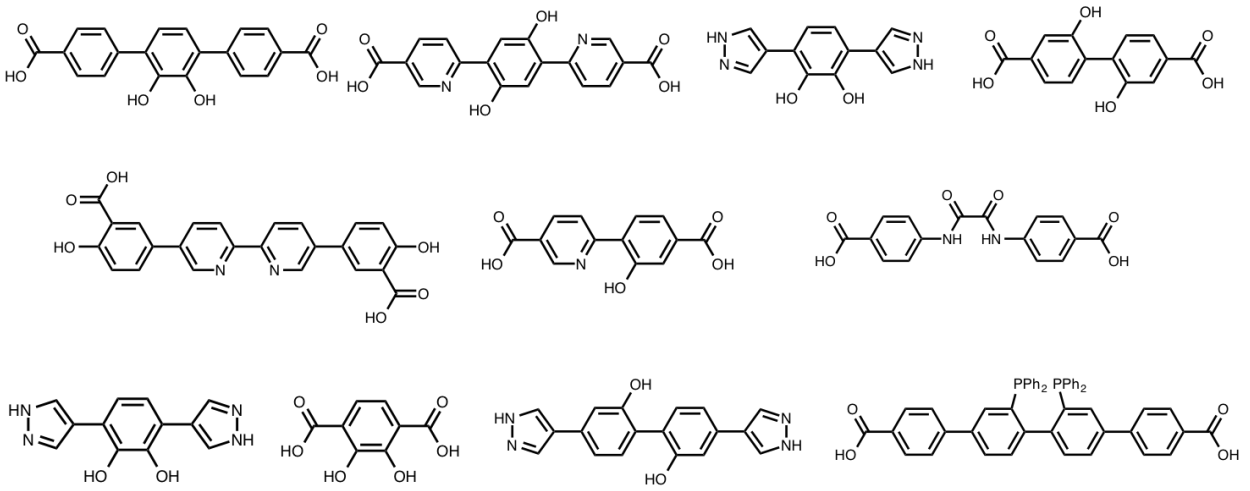

Figure 12. MOF ligands that have been synthesized that contain chelating sites for post-synthetic metalation.

diffraction experiments. However, these experiments proved challenging due to incomplete structural solutions of the D_2-dosed material.

Many new ligands were also prepared for the synthesis of MOFs that would be amenable to post-synthetic metalation. A sampling of these ligands is shown in Figure 12, and one notable example is the catechol-based ligand at the top far left, which was designed for the synthesis of a UIO-68-type MOF (UIO-68[2] is an expanded version of UIO-67 discussed above and exhibits one additional aromatic ring in each ligand). The catechol group in this ligand is promising because it provides both a metal chelation site and charge balance for a divalent metal cation (upon deprotonation), obviating the need for additional charge-balancing anions at the metal center and

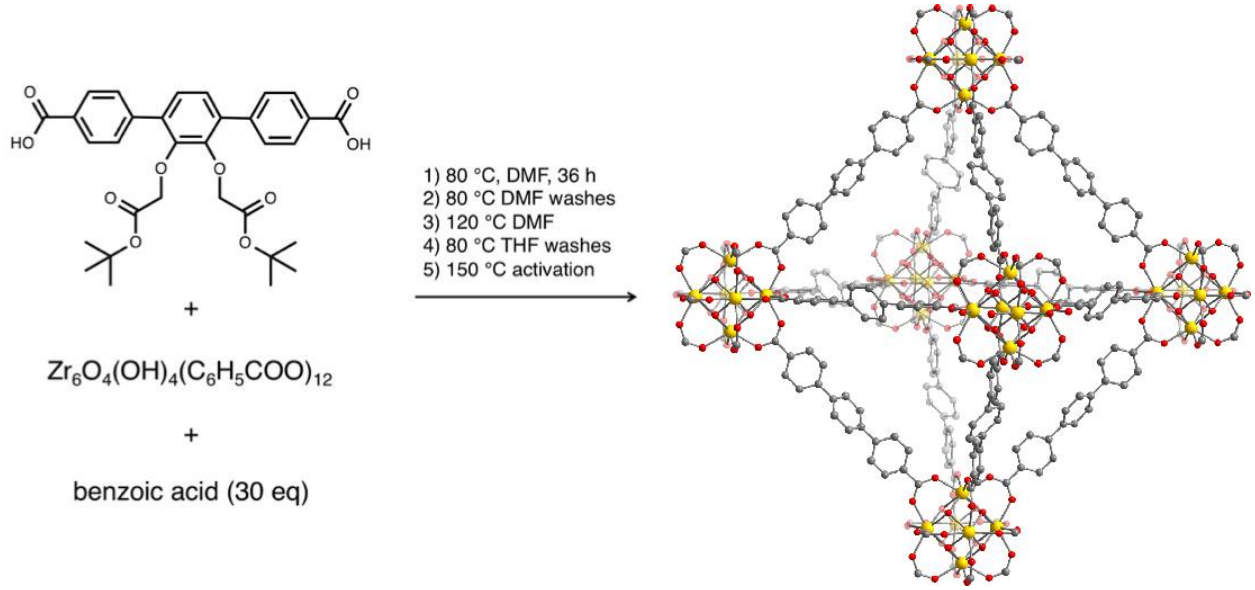

Figure 13. (Left) Synthetic scheme for synthesizing the cat-UIO-68 MOF, including the necessary washes and thermalization of the Boc protecting groups to expose free catechols in the pores of the framework. Activation (step 4) was accomplished by heating at 150 °C under vacuum. (Right) Proposed structure of the catechol MOF with the structure model from single-crystal X-ray characterization of UIO-68 (Reference 2). In the absence of structural characterization, the precise orientation of the catechol groups is not known and hence these groups are not visualized.

potentially exposing additional metal coordination sites. The design of MOFs with such ligands represents a synthetic challenge because a catechol protecting group must be used to prevent metal coordination during framework synthesis, and this group ideally must also be readily removable under conditions to which the MOF is stable. We successfully synthesized such a ligand with Boc protecting groups that can be incorporated into a MOF with the UIO-68 structure type (Figure 13) and subsequently deprotected via thermolysis (decomposition with heating) without loss of framework surface area. The removal of the Boc groups by this route was confirmed by infrared spectroscopy. Continuing work is focused on scaling up the ligand and framework syntheses in order to provide sample material for further metalation with a variety of metal sources. Upon successful isolation of these materials, H_2 adsorption studies will be carried out.

4.2 Task 2: Characterization of Framework-H_2 Interactions

A full structural and dynamics neutron scattering study of Co_2(*m*-dobdc) and Ni_2(*m*-dobdc) was completed over the course of the project. Initial structure determinations of the *m*-dobdc structure came from combined synchrotron X-ray and neutron diffraction analysis. Hydrogen (D_2) locations as a function of loading were determined and insights into the adsorption potential for each of these sites analyzed from inelastic neutron scattering data. Hydrogen diffusion behavior was characterized using quasi-elastic neutron scattering. These results indicated that there are four unique H_2 binding sites within the pores of the M_2(*m*-dobdc) structure type, which can be seen in Figure 14. The most notable result from these studies was that the D_2–M distance is quite short for these materials, only 2.23(5) Å in Co_2(*m*-dobdc) and 2.18(4) Å in Ni_2(*m*-dobdc).

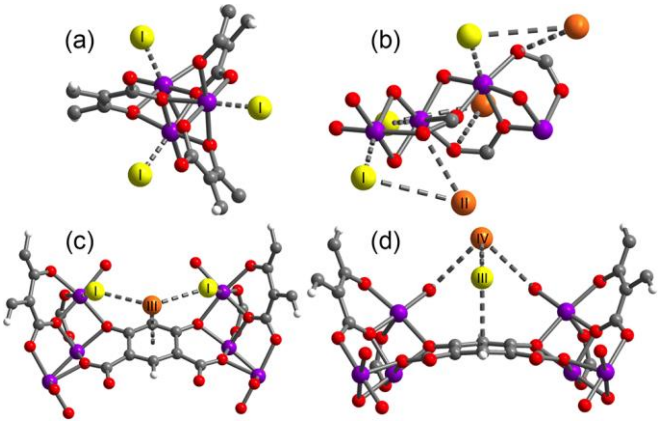

Figure 14. Partial crystal structures obtained at 10 K for Co_2(*m*-dobdc) showing (a) the primary D_2 binding site (site I) on the open metal site; (b) binding site II, interaction with the D_2 in site I; (c) binding site III on the aromatic ring in the linker; and (d) binding site IV, interaction with the D_2 in site III. Purple, gray, red, and white spheres represent Co, C, O, and H atoms, respectively. Yellow and orange spheres represent D_2 molecules.

There is discussion in the literature that an H_2 molecule may elongate at a strong adsorption site, something that we would only consider possible if there was significant electron transfer as in Kubas-type organometallic complexes. We determined that the H_2 molecule does not seem to be elongated, however, in spite of a very short H_2-Co interaction, and the extracted dynamical Debye-Waller factor ($<U^2>$) was consistent between all loadings and rotational modes with a mean value of 0.159(2) $Å^2$, in good agreement with diffraction data (Figure 15).

Importantly, adsorption isotherm data indicated that a D_2 interaction may be slightly stronger than H_2 in certain porous systems. To evaluate the effect of using D_2 compared to H_2 in neutron diffraction experiments, we performed measurements on D_2 and H_2 dosing in Co_2(dobdc) under identical conditions. The quality of the data with H_2 was expected to be poor due to the large incoherent scattering cross-section of H versus D. We determined that this assumption is not

necessarily a difficult reality because the data was compared with Rietveld refinements of the H_2:Co_2(dobdc) system (Figure 16). Summarizing the structural results, the binding sites are the same with an expected slight distance difference Co—D_2 = 2.23(5) Å, Co—H_2 = 2.27(3) Å, implying that the smaller zero-point motion of the heavier isotope (D) may lead to a slightly closer interaction distance, but the overall error bar is dominated by quantum rotations of the molecule.

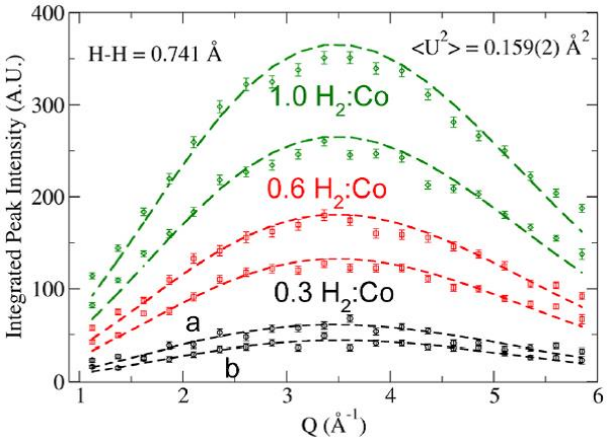

Figure 15. Extracted rotational level areas for different H_2 loadings, fit to a model indicating the classical nature of the adsorbed molecule in Co(*m*-dobdc).

We further determined the structure and locations of hydrogen (D_2) adsorbed in the two-ring, expanded dobdc-type framework, Fe_2(dobpdc). While the isotherms for Fe_2(dobpdc) indicated only a modest increase in Q_{st} compared with Fe_2(dobdc), the D_2–Fe distance in the former was found to be 2.33(6) Å, significantly shorter than the distance of 2.47(3) Å in Fe_2(dobdc), and indicative of quite a high enthalpy of adsorption for hydrogen.

We also initiated efforts to determine hydrogen locations in crystalline materials at much higher temperatures and pressures than typically undertaken. In common practice, specific amounts of gases are dosed in a system and cooled to a few Kelvin. We can probe these systems using neutron diffraction up to 100 bar and at 77 K using both regular data analysis techniques and more specialized approaches that we are still developing. These techniques can be used to effectively determine the packing of H_2 within MOF pores and the uptake of H_2 per unit cell. We

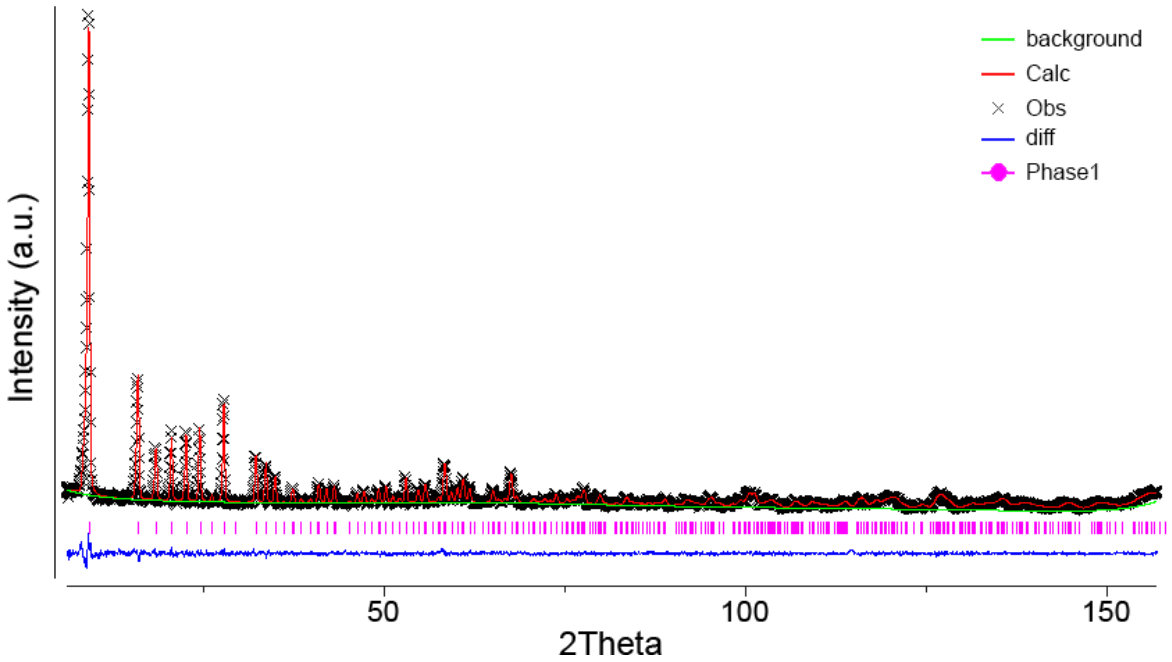

Figure 16. Neutron diffraction data and Rietveld refinement of 0.75 H_2:Co_2(dobdc). The blue difference curve indicates good agreement between the model and the data.

are confident that we can bring these techniques to fruition and standardize the procedure for external use.

4.3 Task 3: First-Principles Calculations of H_2 Binding Enthalpies

The ability to predict suitable materials for H_2 adsorption and the reliable prediction of H_2 binding enthalpies requires a deep understanding of the interactions between the metal site and the adsorbed H_2 molecule. Our approach for the investigation of H_2–metal site interactions in MOFs was to use cluster models that are sufficiently large to describe the adsorption site and its close environment. The geometries and binding enthalpies of H_2 in these clusters were calculated using the latest DFT functionals, which were required for an accurate description of the weak dispersion interactions and strong electrostatic character of H_2 adsorption at a metal site. Beyond absolute energies, which give a single number describing H_2 binding, energy decomposition analysis (EDA) was used to provide qualitative insights into the metal–H_2 interactions, and effectively breaks down the absolute H_2 binding energy into physically-relevant components.

Hydrogen Adsorption in M-BTT and M$_2$(*m*-dobdc)

DFT methods were used as a platform for simulating H_2 binding at open metal sites in the M-BTT MOFs. The calculations were performed starting with the model cluster $[M_4Cl(tz)_8]^-$ (M = Mn, Cu, Zn; tz^- = 5-H-tetrazolate) shown in Figure 17. This cluster can be considered as a truncated portion of the full M-BTT structure, representing a single tetranuclear metal cluster and its ligand coordination sphere. Bond lengths and angles calculated for $[Mn_4Cl(tz)_8]^-$ and $[Cu_4Cl(tz)_8]^-$ using the ωB97X-D functional were found to correlate well with the experimental structures of activated Mn- and Cu-BTT obtained from powder neutron diffraction data.

Hydrogen was introduced into the calculation following the optimization of the bare-cluster geometry. As shown in Figure 17b-d, three different cases of H_2 binding were considered, wherein the H_2 was confined to site I or II only (Figure 17b and c, respectively), or allowed to adsorb at both sites (Figure 17d). A close inspection of the results for the H_2-bound complexes reveals a relatively large difference in the adsorption energies between sites I and II (see Table 2). The difference is pronounced in the case of Mn, for which site I exhibits an H_2 binding energy of −17.2 kJ/mol, compared to just −7.5 kJ/mol for site II. The binding strengths of the two sites are significantly closer in energy in the Cu-based model, which is supported by previous neutron diffraction data in which both sites I and II are populated at similar occupancies even for the lowest guest loadings. Despite the similar structural parameters of $[Cu_4Cl(tz)_8]^-$ and $[Zn_4Cl(tz)_8]^-$, the latter exhibits a considerably higher binding energy as expected. In fact, in the case where H_2 was allowed to populate both sites I and II, the Zn compound showed the most promise for binding hydrogen, exhibiting a slightly higher overall affinity for H_2 than

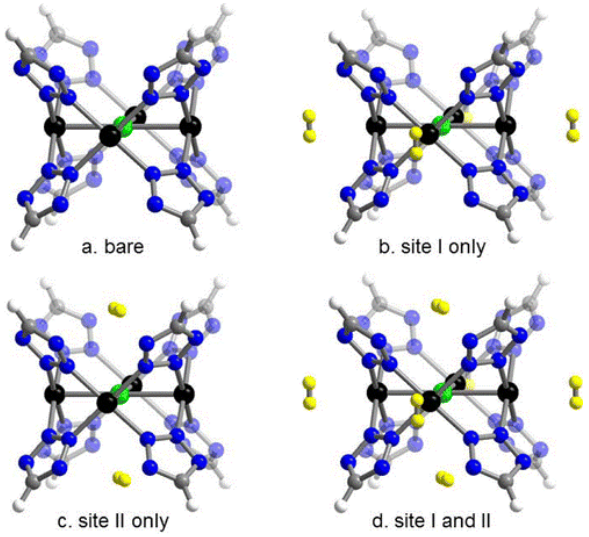

Figure 17. H_2 adsorption in M-BTT.

$[Mn_4Cl(tz)_8]^-$. This high affinity is further reflected in the M–H_2 distances, in which $[Zn_4Cl(tz)_8]^-$ displayed the shortest calculated distance out of the compounds studied. Meanwhile, the Cl···H_2 distances were essentially invariant with the identity of the metal, which is consistent with the calculated site II H_2 binding energies of approximately −7 kJ/mol for each of the three compounds.

Table 2. Calculated H_2 binding enthalpy for M-BTT complexes (units are kJ/mol).

	Mn		Cu		Zn
Site	Calc.	Exp.	Calc.	Exp.	Calc.
Site I	−17.2	−11.9	−10.8	−10.4	−16.3
Site II	−7.5		−7.0		−7.7
Site I + II	−13.6	−10.6	−10.1	−9.8	−14.1

Further calculations were carried out to determine the binding enthalpies as a function of the anion in the cluster. As seen in Figure 18, the cluster expands as the anion size increases from F^- to Cl^- to Br^- to the extreme case with no anion present. Although the metal cations become less electronegative as the cluster expands, they are also projected further into the pore, which strengthens interactions with H_2.[3]

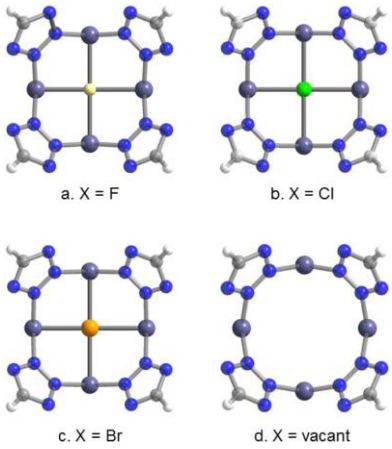

Figure 18. Structural differences as a function of anion in the ZnBTT structure.

Investigation of M_2(dobdc) and M_2(*m*-dobdc) provided another demonstration of the power of our DFT methods to calculate and rationalize H_2 adsorption. As discussed above, these two MOFs were found experimentally to have different H_2 adsorption enthalpies in spite of their similar structures. DFT was used to examine the differences in the electronic structures at the open-metal sites by using cluster models for the M_2(dobdc) and M_2(*m*-dobdc) frameworks. The model used included the metalated linker coordinated to two Co^{2+} centers, while the remaining ligands on each Co^{2+} ion were truncated as formaldehyde molecules in order to maintain charge balance (Figure 19).

The key differences between these two MOFs were rationalized using EDA. In particular, the increased H_2 adsorption affinity of the *m*-$dobdc^{4-}$ material was found to be related to an increased charge transfer and polarization, accompanied by a partially off-setting increase in the energetically unfavorable steric (frozen) interaction, due to the shorter Co···H_2 distance relative to the $dobdc^{4-}$ material. The increased charge-transfer energy of H_2 binding in the *m*-$dobdc^{4-}$ structure was found to be a key contributor to the enhanced binding enthalpy, as this was the largest term in the total calculated binding energy.

For both *m*-$dobdc^{4-}$ and $dobdc^{4-}$ materials, the largest portion of the charge transfer comes from the H_2 σ orbital to the unoccupied orbitals of the Co complex. The increased H_2-to-Co forward donation is indicative of more positive charge at the metal cation in the *m*-$dobdc^{4-}$ complex as compared with the $dobdc^{4-}$ complex. This result aids in rationalizing the experimentally-determined increase in H_2 binding enthalpy for the M_2(*m*-dobdc) frameworks compared with their M_2(dobdc) analogues, as an increased positive charge at the metal center leads to stronger polarization of the bound H_2. Interestingly, our calculations also revealed a difference in the location of the bound H_2 relative to the linker in the two complexes. In the $dobdc^{4-}$ complex the H_2 binds to create a nearly octahedral geometry around the Co^{2+} ion, and sits at a distance of 3.30 Å from the aromatic carbon bound to the carboxylate group (the α carbon). Conversely, in the *m*-$dobdc^{4-}$ complex the H_2 is reoriented toward the linker at a distance of 2.64 Å from the α carbon. This difference suggests that a change in the charge at the α carbon due to the different symmetry of the *m*-$dobdc^{4-}$ linker possibly facilitates a change in

the binding geometry for H_2.

The orbital interactions between H_2 and the Co complexes provided further insight into the stronger H_2 binding in Co_2(*m*-dobdc). While increased forward bonding reflects increased charge density at the metal center, the nature of the back bonding from the complex to H_2 is quite different. In the dobdc^{4-} complex the occupied orbital is primarily localized on the metal center, while in the *m*-dobdc^{4-} species the donating orbital includes contributions from the π system of the linker (Figure 19). This increased back bonding for *m*-dobdc^{4-} agrees with the experimentally-determined red shift observed in the H_2 infrared spectra for the M_2(*m*-dobdc) frameworks, as increased back bonding will weaken the H–H bond. This suggested extra interaction with the linker in the *m*-dobdc^{4-} complex, coupled with greater forward donation of the H_2 to the more positively charged metal center, were found to be the key differences between these two systems that aided in rationalizing the stronger H_2 binding seen in M_2(*m*-dobdc) versus M_2(dobdc).

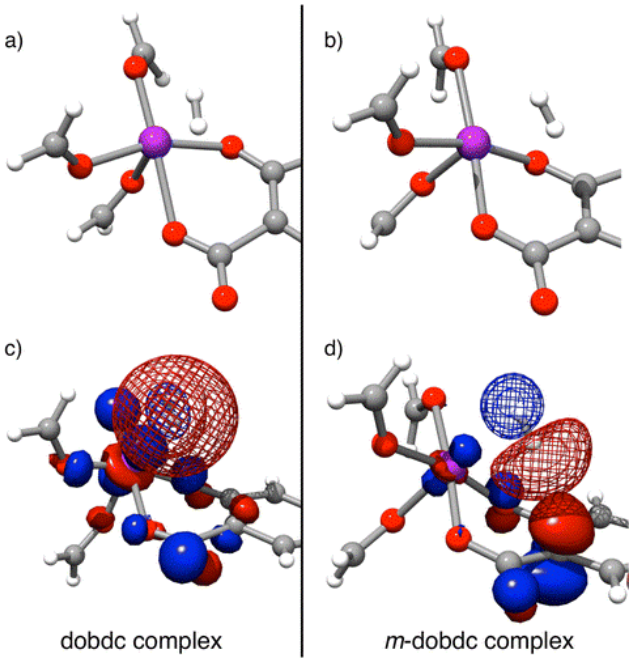

Figure 19. Panels (a) and (b) present the optimized biding geometry. Panels (c) and (b) show the back-bonding charge transfer, which is more localized in the *m*-dobdc^{4-} analogue.

Physical Adsorption of Hydrogen

Weakly adsorbing metalated linkers. We also investigated H_2 physisorption using models representative of realistic framework systems. The three metalated linker-like complexes that were evaluated (Figure 20) are iso-structural to MOF linkers that have been reported in the literature. They were predicted here to be weak H_2 adsorbents, and thus inadequate for practical storage applications. The EDA on these systems provided values for the frozen energy, polarization, and charge transfer that constitute the overall binding energy. These values are given in Table 3 along with the total binding energy and enthalpy. The H_2 adsorption enthalpy for Ti^{IV} and Cu^{II} is approximately −4 kJ/mol, which is a small value and corresponds with the expected adsorption energy of a benzene molecule. In contrast PCM_{18}-$NiCl_2$ exhibits

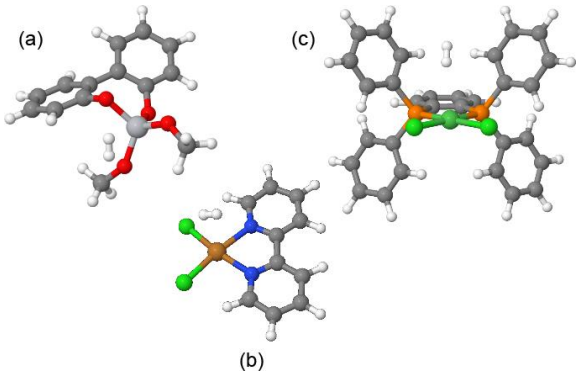

Figure 20. Weakly-interacting complexes of H_2 with metalated linkers: (a) Biphenyl-(TiO_4)-dimethyl (biPh-TiO_4) (b) bpy-$CuCl_2$ (c) PCM_{18}-$NiCl_2$.

Table 3. Energy decomposition analysis of H_2 binding to the complexes given in Figure 17 (units are kJ/mol).

	biPh-TiO_4	**bpy-$CuCl_2$**	**PCM_{18}-$NiCl_2$**
Frozen	−2.4	−0.8	−1.7
Polarization	−0.8	−1.9	−2.2
Charge Transfer	−1.5	−2.8	−4.8
Total ΔE	−4.7	−5.5	−8.7
ΔH_{ads}	−3.6	−4.4	−7.9

a much higher adsorption enthalpy of about −8 kJ/mol. Notably this species has a somewhat stronger charge-transfer interaction with the H_2 molecule, which results from charge contribution from the aromatic rings (surrounding the adsorption site above the metal) into Rydberg-like orbitals of the H_2. This result clearly demonstrated that the mere existance of an exposed site is not a sufficient condition for strong H_2 adsorption.

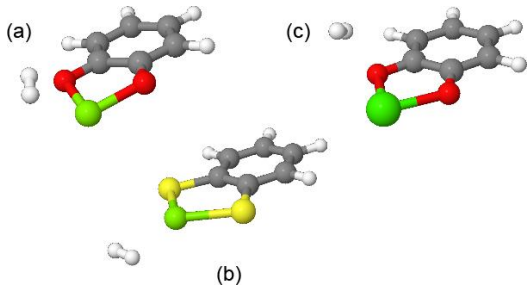

Figure 21. Complexes exhibiting a strong H_2 physisorption interaction: (a) catechol-Mg (cat-Mg) (b) catechol-Ca (cat-Ca), and (c) 1,2-benzenedithiol-Mg (BDT-Mg).

Table 4. Energy decomposition analysis of H_2 binding to the complexes given in Figure 18 (units are kJ/mol).

	cat-Mg	cat-Ca	BDT-Mg
Frozen	−1.8	2.1	−1.3
Polarization	−11.1	−16.0	−7.7
Charge Transfer	−6.7	−9.1	−6.1
Total ΔE	−19.6	−23.0	−15.1
ΔH_{ads}	−18.9	−18.6	−11.1

Strongly adsorbing metalated linkers. We further examined metalated-linker models that are predicted to bind H_2 more strongly via "physical" interactions and analyzed the conditions that give rise to such a situation. The linkers were based on the catechol functionality discussed in Section 4.1 and the sulfur analog, 1,2-benzenedithiol. These ligands were shown to be capable of forming highly polar metal coordination complexes with stronger H_2 adsorption properties than those discussed above. The optimized structures of the complexes are shown in Figure 21. To trace the origin of this strong interaction of the catechol complexes with H_2, EDA was again carried out and the results are given in Table 4. Interestingly, the catechol-metalated units were found to exhibit a much stronger polarization interaction with H_2 than the weakly adsorbing species discussed above, resulting from a greater ability of the catechol species to induce electrostatic moments in the H_2 molecule.

4.4 Task 4: High-Pressure H_2 Adsorption Measurements

High-pressure H_2 adsorption measurements are another important characterization of novel materials of interest for use in vehicle storage of H_2 gas. A substantial effort in the high-pressure area of this project was to pioneer the development of a novel apparatus that could be widely used for a range of adsorbents to reliably test for H_2 adsorption over many cycles and for multiple temperatures. A custom-made, high pressure volumetric Sieverts' apparatus (operating at ambient temperature and pressures up to 350 bar) was used for this purpose (Figure 22). For calibration and validation of the system and the data acquisition

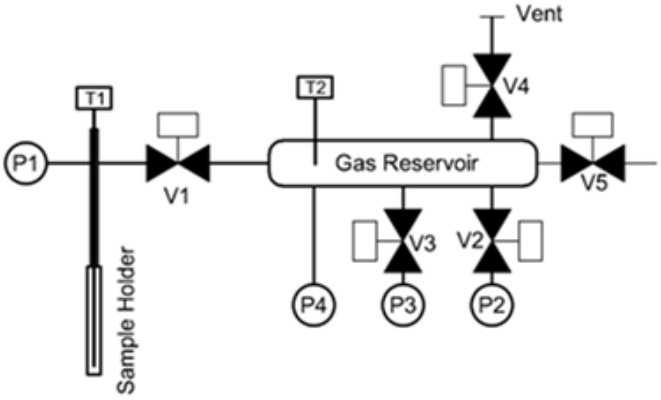

Figure 22. High pressure Sievert system plumbing and instrumentation, where P = pressure transducer, T = thermocouple and V = pneumatic valve.

procedure, we measured the H_2 adsorption of several benchmark materials including activated carbons and Zn-based frameworks such as MOF-177. Adsorption data for MOF-177 was measured both at room temperature and 40 °C in preparation for the comprehensive measurements that would be performed on novel frameworks made in this project.

We found our room temperature results to be in good agreement with low-pressure literature data, and found no apparent correlation between N_2 adsorption-based surface areas and excess H_2 adsorption at ambient temperature. For example, MOF-177 displays a maximum uptake that is just over half of that for the activated carbons in spite of its larger surface area. We also determined the importance of measuring large sample sizes when possible (200-500 mg) and established a method for calculated adsorption enthalpies from room temperature and 40 °C data. Following this verification, we further modified the high-pressure apparatus to measure multiple cycles on the systems of interest in this project (e.g., M_2(dobdc), M_2(dobpdc), and M_2(*m*-dobdc)).

High-Pressure Adsorption for M_2(dobdc) and Analogues

Hydrogen adsorption isotherms were measured at ambient temperature for Ni_2(dobdc), Ni_2(dobpdc), and the cobalt version of the three-phenyl-ring analogue, Co_2(dotpdc). This data revealed that linker expansion is correlated with a greater adsorption of hydrogen per unit cell. However, the data for Ni_2(dobpdc) and Co_2(dotpdc) more or less overlay with each other, suggesting that either subsequent linker expansion does not play a significant role in the ambient temperature adsorption or that the binding energy for Co_2(dotpdc) is lower than Ni_2(dobpdc). We also carried out high-pressure measurements on samples of Ni_2(*m*-dobdc) and Co_2(*m*-dobdc) and compared these data with the parent Ni_2(dobdc), Ni_2(dobpdc), and Co_2(dotpdc). Notably Ni_2(*m*-dobdc) and Ni_2(dobdc) exhibit identical excess adsorption in spite of their structural dissimilarities (Section 4.1). A comparison of the excess adsorption for Ni_2(dobdc), Ni_2(dobpdc), Co_2(*m*-dobdc), and Co_2(dotpdc) (Figure 23, left) revealed that for Co as well as Ni, the expanded frameworks exhibit a higher excess adsorption. Adsorption enthalpies were calculated using a method based on the Dubinin-Astakov (DA) model (see *Am. J. Anal. Chem.* publication under Section 5). This model is accurate for the adsorption of supercritical gases at high pressure or for subcritical, multilayer adsorption, and differs from the Clausius-Clapeyron method in that only

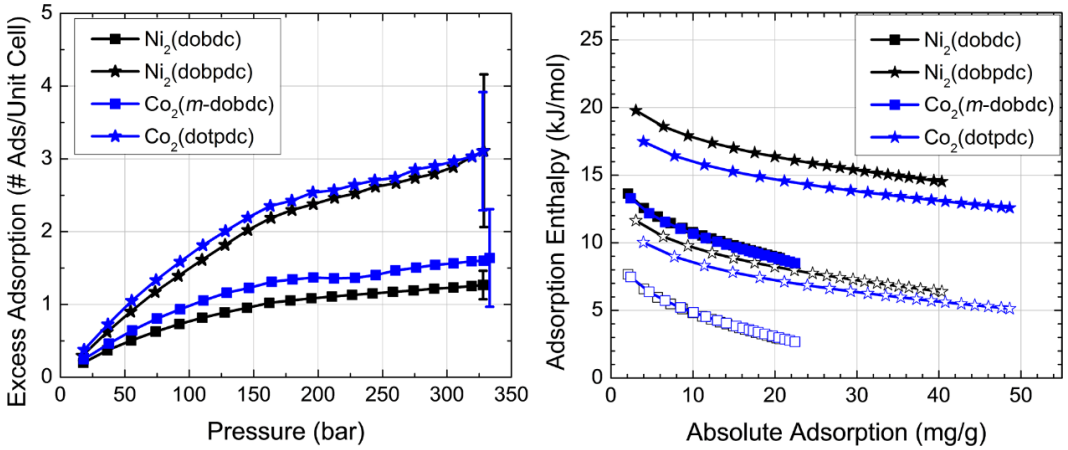

Figure 23. (Left) Ambient temperature hydrogen excess adsorption per unit cell for the nickel and cobalt Ni_2(dobdc) and Co_2(*m*-dobdc) (square symbols) with the two-ring (dobpdc) and three-ring (dotpdc) expanded analogues (star symbols). (Right) Plot of adsorption enthalpies (calculated using the Dubinin-Astakhov isotherm) versus absolute adsorption. The solid symbols represent ambient temperature enthalpies and open symbols represent 0 K enthalpies.

one isotherm is necessary to calculate the adsorption enthalpy. To briefly summarize the method, we apply the DA model directly to a form of the van't Hoff equation:

$$\Delta\dot{h}_{\text{ads}} = R\left(\frac{\partial \ln[f]}{\left(\frac{1}{T}\right)}\right)_{\theta}$$

where f is the fugacity, T is the temperature, R is the gas constant, and the derivative is taken at constant coverage, θ. The fugacity is used in lieu of the pressure to account for non-ideality of the gas. For the DA model, the enthalpy is:

$$\Delta\dot{h}_{\text{ads}} = E\ln\left[\frac{m_0}{m_{\text{abs}}}\right]^{\frac{1}{\xi}} + \gamma RT$$

where E, m_o, γ, and ξ are empirical constants and m_{abs} is the absolute adsorption as a function of fugacity.

There are couple of important observations regarding enthalpies calculated in this way. First, the enthalpy here is temperature dependent, so there is a corresponding zero-temperature enthalpy, $\Delta\dot{h}_0 = \Delta\dot{h}_{\text{ads}}(T=0)$, which is more indicative of the actual gas-solid interaction. Second, because these enthalpies are being measured at ambient temperature, they will appear to be higher than those measured at cryogenic temperatures, even though the gas-solid interaction energy is the same (note Figure 23, right). We also note that the DA model does not satisfy Henry's law, which means that the calculated enthalpies are only valid at higher coverage. Adsorption enthalpies calculated in this way corroborated the excess adsorption per unit cell data (Figure 23, right), and samples with more hydrogen adsorbed per unit cell also exhibited higher adsorption enthalpies. Due to a change in project emphasis requested by the program managers, no further analysis or studies were possible to further elucidate these results.

Through additional studies on the promising Ni_2(*m*-dobdc) material discussed in Section 4.1, we confirmed the ability of our apparatus to measure H_2 adsorption for 10 cycles at room temperature and 40 °C, which is a more relevant temperature for on-board vehicle applications. Within the error of the measurement, the adsorption of Ni_2(*m*-dobdc) did not diminish over the 10 cycles, which was a promising result for the prospect of on-board vehicle storage of H_2. Following these results, there was a change in emphasis within the project to more heavily target the synthesis of new materials, and thus further high-pressure studies were discontinued.

4.5 Conclusions

Many new adsorbents were explored in this project via both modification of known metal-organic frameworks (e.g., M_2(dobpdc) and M_2(*m*-dobdc)) and the development of new synthetic strategies geared toward significantly increasing the density of H_2 that can be stored in these materials. A significant portion of the effort in this project was directed toward the rigorous characterization of the promising M_2(*m*-dobdc) frameworks and other targets, and these efforts

were strongly supported by collaborative characterization and computational efforts. Going forward, the research progress made here suggests that in order to significantly increase the volumetric H_2 storage capacity within MOFs and to approach the DoE targets, current materials must be tuned and new materials optimized to incorporate a maximum number of open metal coordination sites. It is at these sites that H_2 binds most strongly, and thus increasing open metal site density will increase the capacity of a given material for H_2 while optimizing volumetric uptake for future applications. We believe the most promising strategy in this regard will be to pursue MOFs with catechol linkers, wherein secondary metal cations can be installed that are capable of binding multiple H_2 per metal center, thereby effectively increasing open metal site density. Here, even though the total given pore volume would decrease with these modifications, the capacity for H_2 should substantially increase for appropriate structures. Empirical analysis of the well-known MOF-5 ($Zn_4O(bdc)_3$, bdc^{2-} = 1,4-benzenedicarboxylate, Figure 24) illustrates this strategy well.

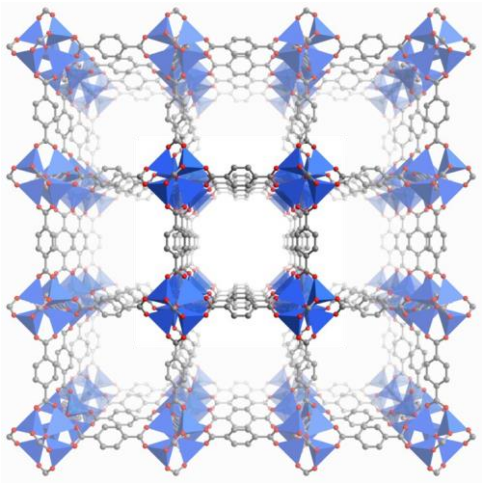

Figure 24. Highlighted view of one of the square pores in MOF-5.

At 298 K, this framework exhibits an H_2 uptake of only 10 g/L, much lower than the target minimum 40 g/L at room temperature. In order to achieve this storage target, it is necessary to store at least 12 H_2 molecules per 1000 $Å^3$ of empty pore space in a MOF.[4] For simplicity we consider a single cube of MOF-5, which has a total cube volume of 2144 $Å^3$ wherein therefore we would like to store at least 26 H_2 molecules. In order to successfully achieve this target capacity, each H_2 molecule should then take up no more than ~83 $Å^3$ of free space.

The actual free volume in the MOF-5 cube is only 77% of this total volume,[5] ~1651 $Å^3$, based on the single crystal density, and thus an even stricter requirement is placed that each H_2 molecule should take up no more than ~63 $Å^3$ of free space. Upon replacing the bdc^{2-} linkers with catechol ligands and installation of Ca^{2+} ions, the free volume reduces to 1329 $Å^3$. However, assuming that each two-coordinate Ca^{2+} is capable of binding 4-6 H_2 molecules to satisfy its coordination sphere, it is still possible to adsorb at least 26 H_2 molecules, each taking up a minimal ~51-28 $Å^3$ of space, resulting in impressive capacity ranging from 38-

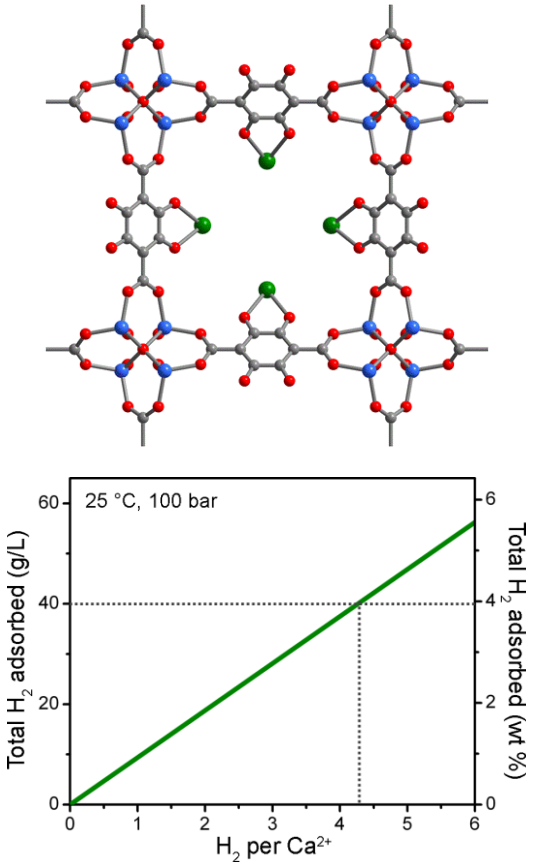

Figure 25. (Top) Pictorial representation of a face of the modified MOF-5 structure with catechol-based ligands and coordinated Ca^{2+} ions. (Bottom) Estimated H_2 capacity of this material dependent on number of H_2 molecules bound to Ca^{2+}.

56 g/L (Figure 25). While these observations remain empirical, they stress the promise in targeting the proposed strategy.

Although this effort is synthetically non-trivial as discussed above, the research accomplished in this project has made significant strides in the development of the synthetic tools and characterization/computational methods that will continue to be invaluable in further evaluation of new materials for H_2 storage and ultimately achieving the storage targets established by the DoE.

4.6 References

(1) Cheon, Y. E.; Suh, M. P.; *Chem. Commun.* **2009**, 2296.

(2) Cavka, J. H.; Jakobsen, S.; Olsbye, U.; Guillou, N.; Lamberti, C.; Bordiga, S.; Lillerdu, P. *J. Am. Chem. Soc*. **2008**, *130*, 13850.

(3) Sumida, K.; Stück, D.; Mino, L.; Chai, J.-D.; Bloch, E. D.; Zavorotynska, O.; Murray, L. J.; Dincă, M.; Chavan, S.; Bordiga, S.; Head-Gordon, M.; Long, J. R. *J. Am. Chem. Soc.* **2013**, *135*, 1083.

(4) This assumes strong binding sites with adsorption enthalpies ranging from 15-20 $kJ \cdot mol^{-1}$ and an entropy of adsorption that ranges from $8.5 \cdot R$ to $10 \cdot R$, where $R = 8.314\ J \cdot mol^{-1} \cdot K^{-1}$ is the ideal gas constant. Compare with Ni_2(*m*-dobdc), which can store 5 H_2 per 1000 $Å^3$, assuming one molecule per Ni^{2+}, or 21 H_2 molecules per 1000 $Å^3$ for liquid H_2. The above empirical estimates and analysis were provided by Dr. Jarad A. Mason, PhD Long group 2015.

(5) Based on pore volume and single crystal density.

5 Project Output

A. Journal Articles

1. K. Sumida, D. Stuck, L. Mino, J.-D. Chai, E. D. Bloch, O. Zavorotynska, L. J. Murray, M. Dincă, S. Chavan, S. Bordiga, M. Head-Gordon, J. R. Long,, "Impact of Metal and Anion Substitutions on the Hydrogen Storage Properties of M-BTT Metal-Organic Frameworks" *J. Am. Chem. Soc.* **2013**, *135*, 1083–1091.
2. R. Ameloot, M. L. Aubrey, B. M. Wiers, P. Gomora-Figueroa, S. N. Patel, N. P. Balsara, J. R. Long, "Lithium Ion Conductivity in the Metal-Organic Framework UIO-66 via Dehydration and Insertion of Lithium *t*-Butoxide" *Chem., Eur. J.* **2013**, *19*, 5533–5536.
3. C. M. Brown, A. J. Ramirez-Cuesta, J.-H. Her, P. S. Wheatley, R. E. Morris, "Structure and spectroscopy of hydrogen adsorbed in a nickel metal-organic framework" *Chem. Phys.* **2013**, *427*, 3–8.
4. M. Beckner, A. Dailly, "Adsorption Enthalpy Calculations of Hydrogen Adsorption at Ambient Temperature and Pressures Exceeding 300 bar" *Am. J. Anal. Chem.* **2013**, *10C*, 8–16.
5. M. L. Aubrey, R. Ameloot, B. M. Wiers, J. R. Long, "Metal-Organic Frameworks as Solid Magnesium Electrolytes" *Energy Environ. Sci.* **2014**, *7*, 667–671.
6. R. A. Pollock, J.-H. Her, C. M. Brown, Y. Liu, A. Dailly, "Kinetic trapping of D_2 in MIL-53(Al) observed using neutron scattering" *J. Phys. Chem. C* **2014**, *118*, 18197–18206.
7. M. T. Kapelewski, S. J. Geier, M. R. Hudson, D. Stuck, J. A. Mason, J. N. Nelson, D. J. Xiao, Z. Hulvey, E. Gilmour, S. A. FitzGerald, M. Head-Gordon, C. M. Brown, J. R. Long, "M_2(*m*-dobdc) (M = Mg, Mn, Fe, Co, Ni) Metal-Organic Frameworks Exhibiting Increased Charge Density and Enhanced H_2 Binding at the Open Metal Sites" *J. Am. Chem. Soc.* **2014**, *136*, 12119–12129.
8. E. Tsivion, J. R. Long, M. Head-Gordon, "Hydrogen Physisorption on Metal–Organic Framework Linkers and Metalated Linkers: A Computational Study of the Factors That Control Binding Strength" *J. Am. Chem. Soc.* **2014**, *136*, 17827–17835.
9. D. Gygi, E. D. Bloch, J. A. Mason, M. R. Hudson, M. I. Gonzalez, R. L. Siegelman, T. A. Darwish, W. L. Queen, C. M. Brown, J. R. Long, "Hydrogen Storage in the Expanded Pore Metal-Organic Frameworks M_2(dobpdc) (M = Mg, Mn, Fe, Co, Ni, Zn)." *Submitted.*

Presentations, Conference Papers, or Public Releases of Results

1. C. M. Brown, "Understanding adsorption in porous materials through structure and spectroscopy", American Chemical Society National Meeting, April 7, 2013, New Orleans, LA.
2. Z. Hulvey, C. M. Brown, "Neutron Powder Diffraction: D_2 vs H_2", IAEA Experts Meeting, December 2013, Key Largo, FL.
3. M. Beckner, A. Dailley, "High-pressure, ambient temperature hydrogen storage in metal-organic frameworks and porous carbon", APS Meeting, March 2014, Denver, CO.
4. C. M. Brown, "Applications of neutron scattering to understanding structure and gas storage properties of metal-organic frameworks and related materials", Chemistry Seminar, May 8, 2014, Drexel University, Philadelphia, PA.
5. M. Beckner, A. Dailly, "Hydrogen and Natural Gas Storage in Adsorbent Materials for Automotive Applications", Proceedings of the 13th International Conference on Clean

Energy, June 2014, Istanbul, Turkey.

6. C. M. Brown, "Neutron studies of hydrogen in porous materials", Metal-Hydrides Symposium, July 20, 2014, Manchester, UK.
7. C. M. Brown, "Scattering Studies of Adsorbates in Porous Media", American Chemical Society National Meeting, August 10-14, 2014, San Francisco, CA.
8. M. T. Kapelewski, S. J. Geier, M. R. Hudson, D. Stuck, J. A. Mason, J. N. Nelson, D. J. Xiao, Z. Hulvey, E. Gilmour, S. A. FitzGerald, M. Head-Gordon, C. M. Brown, J. R. Long, "Structural Isomer of M_2(dobdc) with Increased Charge Density and Stronger H_2 Binding at the Open Metal Sites", American Chemical Society National Meeting, August 10-14, 2014, San Francisco, CA.
9. C. M. Brown, "Structural Studies of Adsorbates in Porous Media", MOF-2014, September 2014, Kobe, Japan.
10. J. Mason, U.S. Car Hydrogen Storage Tech Team Presentation, September 2014, Detroit, MI.
11. C. M. Brown, "Structural Studies of Adsorbates in Porous Media", Neutron Day, October 30, 2014, University of Maryland.
12. C. M. Brown, "Structural Studies of Adsorbates in Porous Media", Telluride Science Research Center Workshop, June 16, 2015, Telluride, CO.

B. Websites

N/A

C. Networks or collaborations fostered

- A previously existing collaboration with Professor Stephen FitzGerald of Oberlin College was continued as a part of this project. Professor FitzGerald collected H_2-dosed infrared spectra for a variety of materials evaluated as a part of this project, including Ni_2(*m*-dobdc) and Co_2(*m*-dobdc).
- Collaborated internationally with members of the IEA HIA Task 32 "Hydrogen-based Storage Energy"

D. Technologies/Techniques

N/A

E. Inventions/Patent Applications

- Long, J. R.; Kapelewski, M. T.; Geier, S. J. Metal-Organic Frameworks with a High Density of Highly Charged Exposed Metal Cation Sites. Submitted, patent pending.

F. Other Products

N/A

6 Computer modeling

A. Model description

Models used in this work were crafted based on available crystal structures, as obtained experimentally. The geometry and energy of hydrogen adsorption was calculated using density functional theory (DFT) applied to the crystal structure + adsorbed hydrogen model.

B. Performance criteria

The standard criteria for the accuracy of DFT calculations is achieving a "chemical accuracy" of less than 4 kJ/mol with respect to experimental measurements. However, one must consider that experimental measurements have their own intrinsic error, such that actual errors can be higher.

C. Test results

As already mentioned above, the accuracy of the DFT calculations using cluster models was demonstrated for systems where structural data and energies were available, such as for M-BTT, M_2(dobdc) and M_2(*m*-dobdc).

D. Theory

DFT can be considered as a standard tool in computational theory with an already well known theoretical background. The use of cluster models implicitly assumes short-ranged forces dominate the H_2 metal-site interactions.

E. Mathematics

DFT can be considered as a standard tool in computational theory with an already well known mathematical background.

F. Peer Review

DFT is well-known among the theoretical chemistry community and is continuously being developed and improved and as such it is commonly used and peer-reviewed.

G. Hardware requirements

N/A

H. Documentation

N/A